

Experimental investigation of migration and solidification of molten salt leaking through tank cracks^{*}

Hua SHI, Hao ZHOU^{†‡}, Peng-nan MA, Jian-kang WANG, Hao FANG, Jia-wei LUO, Kun-zan QIU

State Key Laboratory of Clean Energy Utilization, Institute for Thermal Power Engineering, Zhejiang University, Hangzhou 310027, China

[†]E-mail: zhouhao@zju.edu.cn

Received Jan. 6, 2021; Revision accepted May 29, 2021; Crosschecked Dec. 5, 2021

Abstract: Molten salt is often used for heat transfer and thermal energy storage in concentrated solar power. Molten salt leakage and migration is a significant issue in its application. Molten salt migration and solidification in thermal porous foundation materials through cracks are experimentally investigated. The impact of factors, including crack length and width, operation temperature, and leakage mass of molten salt, are studied through an experimental device modeling the leakage of the actual molten salt storage tank. Experimental results show that the crack width and length slightly affect the migration depth, but directly affect the shape of the agglomeration of solidified salt and porous foundation material. The most important factor affecting the migration depth of molten salt leaking through cracks is the tank operating temperature. The molten salt migration depth when the operating temperature is 500 °C is 95.8% higher than that with an operating temperature of 300 °C. As the leakage molten salt mass reached 400 g, the average migration width increased by 23.6%, but the migration depth only increased by 5.2%. It is found that the foundation material temperatures after leakage accidents increase with an increase in the mass of leaked molten salt.

Key words: Molten salt; Leaking; Migration; Crack; Foundation material

<https://doi.org/10.1631/jzus.A2100011>

CLC number: TH71


1 Introduction

Molten salt thermal energy storage (TES) technology has developed into one of the most attractive energy storage methods (Prieto et al., 2016a, 2016b), particularly for concentrated solar power (CSP) systems. With the advantages of superior heat transfer performance and large specific heat, high-temperature molten salt is extensively applied to transfer heat and store thermal energy (Janz, 1967; Yuan et al., 2018). However, molten salt brings great thermal shock to its container in the repeated cycle of charging and discharging (Li et al., 2017), while the

molten salt composition has a certain degree of corrosiveness to the material at high temperature. Du et al. (2016) and Xu et al. (2018) studied the fatigue crack and thermal stress of a solar tower receiver of molten salt. Moreover, there is a critical thermal ratcheting phenomenon in a molten salt thermocline energy storage tank (Flueckiger et al., 2011). The thermal stress repeatedly changes during the cycle and operation process, which causes fatigue fracture and cracking of the container at the locations of higher stress or strain. The high-temperature corrosion performance of nitrate and chlorate molten salts on stainless steels has been studied (Gomes et al., 2019; Sun et al., 2020). Both Crescent Dunes Power Station (USA) and Gemasolar Thermosolar Plant (Spain) have had the cases of molten salt leakage (Wan et al., 2020). The leaking molten salt migrates to the tank foundation and the soil, and even causes pollution of the groundwater.

[‡] Corresponding author

^{*} Project supported by the National Natural Science Foundation of China (No. 52036008)

 ORCID: Hao ZHOU, <https://orcid.org/0000-0001-9779-7703>

© Zhejiang University Press 2021

At present, the research on leakage and migration mainly focuses on pure gas or liquid substances, such as hydrogen, natural gas, and petroleum (Huang et al., 2013). Vialle et al. (2016) developed the flow and transport research of carbon dioxide leakage through the fractured caprock of a storage reservoir. Bremer et al. (2014) created the sensor concept combining the fiber Bragg grating-based humidity sensor and the swellable polymeric sensor to investigate the leakage of the sewage tunnel. However, the leakage process of molten salt involves the leakage and diffusion of the high-temperature liquid that undergoes phase change and solidification after it transfers heat to the surrounding objects. Weisbrod et al. (2004) demonstrated that the seepage speed of saline solutions was affected primarily by an induced surface tension, and the density was not the primary factor in the seepage patterns. Zafari et al. (2015) and Ou et al. (2017) investigated the transport properties and heat transfer of porous metal foams by the method of microtomography images. In recent years, researchers have investigated the molten salt flow and thermal characteristics in different heat exchange tubes and in porous media of thermocline storage tanks. Lu et al. (2013) and Yao et al. (2018) researched the convective heat transfer performance of molten salt when it flows through a shell-and-tube heat exchanger and a transversely grooved tube, respectively. Abdulla and Reddy (2017) created an integrated transient 2D two-phase model of a thermocline TES tank and found that, relative to the molten salt inlet velocity, the operation temperature limit more significantly affects the discharging efficiency of the thermal storage system. The cycling characteristics of the packed bed TES system with molten salt and cascaded phase-change material capsules were researched by Wu et al. (2016), including the temperature distribution between the packed capsules and the molten salt, the variation of the outlet temperature, and the cumulative efficiency of cascaded cycles. Based on multi-scale experiment and local thermal equilibrium theory, Yin et al. (2017) studied the hybrid thermocline charging/discharging process in a porous packed bed tank and concluded that the thermal storage device structure, rather than the thermal storage conditions and operational approach, is the most important factor affecting effective thermal

storage capacity. Yang et al. (2016) experimentally researched the temperature gradient variations of a molten salt thermocline storage tank with a filler material of ceramic particles. The thermal storage capacity was found to decrease continuously with increasing charging time. Moreover, some research studied heat transfer and the phase change dynamics process by combining the volume of fluid model and the continuum surface force model when molten salt fills into cold receiver tubes. Lu et al. (2010) revealed the evolution behavior of molten salt freezing and melting phenomena in cold filling by numerical simulation. The effects of wall temperature and residual flow on filling and solidification were examined by Im et al. (2001). The detailed mechanism of solidification/melting and the evolution of the pressure and temperature drop along the tube were demonstrated by Liao et al. (2014). Wu et al. (2017) and Zhang et al. (2019) investigated the transport and heat transfer process of nitrate salt leaking into cold porous materials and studied the variation of diffusion trends under different conditions.

An important issue for molten salt application is molten salt leakage and transport in porous material with solidification. However, there has been little experiment and mechanism research of molten salt migration in cold sand or soil. The present work experimentally studies the migration characteristics of molten salt leaking into thermal steady-state foundation materials through storage tank cracks. The migration range is measured under different conditions, including the crack dimensions, operation temperature, and mass of leaking molten salt. The study can guide the environmental polluted management and leakage detection of high temperature storage tanks.

2 Materials and methods

2.1 Materials

Solar salt, a mixture of 60% (in weight) sodium nitrate and 40% potassium nitrate, was used in the experiments. The salt was supplied by Zhejiang Lianda Chemical Company Limited, China. The molten salt mixture can be used from 260 °C to 600 °C, and its thermophysical properties in a liquid state are

shown in Table 1 (Ferri et al., 2008; Zhou et al., 2020b). The salt has an initial melting temperature of 219.8 °C and a phase change latent heat of 113 kJ/kg (Chieruzz et al., 2017). The usual molten salt tank foundation structure is multilayer insulating materials and concrete base slab with a ventilating system at the bottom (Bonilla et al., 2018). Light expanded clay aggregate (LECA) is applied as the thermal insulation material in the tank foundation to reduce the heat loss through the foundation (Zhou et al., 2020a). The characteristics of particle sizes, packed bulk density, and porosity are given in Table 2 (Zhou et al., 2020b).

Table 1 Properties of solar salt in a liquid state (Ferri et al., 2008; Zhou et al., 2020b)

Parameter	Description
Specific heat capacity, c_p (J/(kg·K))	$1443+0.172T$
Density, ρ (kg/m ³)	$2090-0.636T$
Thermal conductivity, λ (W/(m·K))	$0.443+0.00019T$
Viscosity, μ (kg/(m·s))	$2.2714 \times 10^{-2} - 1.2 \times 10^{-4}T$ $+ 2.281 \times 10^{-7}T^2$ $- 1.474 \times 10^{-10}T^3$

T is the temperature of molten salt in °C

Table 2 Parameters of LECA (Zhou et al., 2020b)

Parameter	Value
Particle size ratio (%)	
3.35–6.30 mm	39
6.30–8.00 mm	31
8.00–10.00 mm	13
10.00–20.00 mm	17
Bulk density (kg/m ³)	373.5
Porosity (%)	43.3

2.2 Methods

As shown in Fig. 1, the experimental devices for investigating molten salt leaking and migration in thermal state materials include an electrical resistance heater equipped with a lifting device, a temperature controlling device, a test rig with thermal insulation material layer, a muffle furnace, thermocouples, and a data acquisition instrument. The electrical resistance heater produces the thermal performance from the high-temperature medium in the storage tank to the foundation material at the bottom. The range of

temperature is 30–800 °C and the resolution is ± 1 °C. A muffle furnace heats the salt to the operating temperature with a resolution of ± 1 °C. The foundation material is stacked in the test rig, and the thickness of the firebrick insulation layer is 150 mm. The temperature distribution and evolution process of migration and solidification are measured and recorded by thermocouples and data acquisition equipment. The accuracy of the thermocouples is ± 0.1 °C, and the gauging points are located at central positions with a height interval of 40 mm.

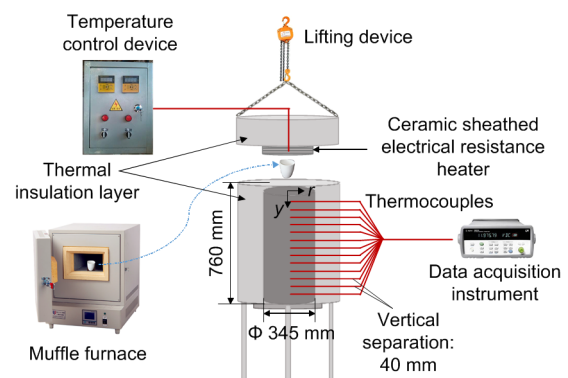


Fig. 1 Experimental system of molten salt leakage and migration in hot foundation materials. Reprinted from (Zhou et al., 2020b), Copyright 2020, with permission from Elsevier

Before the leaking process, the foundation material LECA, graded according to the proportions in Table 2, was heated by the electrical resistance heater. When the temperature difference of the foundation material was less than 0.5 °C within 3 h, it was assumed that the foundation material had reached a thermal steady state. The salt was heated to the operating temperature in a muffle furnace and kept at a constant temperature for 5 h to make its temperature distribution uniform. The molten salt temperature was the same as the heater temperature, which represented the operating temperature of the thermal storage tank. Then, the heater was pulled up, and the molten salt was poured into a quartz crucible placed on the top of the foundation material. Slots of various sizes were cut in the quartz crucibles to simulate the cracks found in practice. When the leakage of molten salt was completed, the heater was kept at a constant temperature, and the molten salt migration and solidification process was still detected until the

temperature of the foundation material LECA attained another steady state. Then the heater stopped heating, and the foundation material with salt was naturally cooled to room temperature, the agglomeration of LECA and salt was taken out, and the transport ranges were measured with an accuracy of ± 1 mm. The experimental conditions of tested cases are given in Table 3 (Zhou et al., 2020b), and images of the leaking crucibles are shown in Fig. 2. The tests in cases A1–A4 and B1–B3 studied the effect of slot width and length on the molten salt leaking and migration, respectively. Compared with case A2, cases C1–C3 were conducted at higher operating temperatures, and cases D1 and D2 have different leaking molten salt masses. The effects of the four factors on the leakage and migration process are studied separately.

Table 3 Experimental conditions of tested cases (Zhou et al., 2020b)

Case	Operating temperature (°C)	Length of leaking slot (mm)	Width of leaking slot (mm)	Mass of leaking molten salt (g)
A1	300	30	3	600
A2	300	30	5	600
A3	300	30	7	600
A4	300	30	10	600
B1	300	5	5	600
B2	300	10	5	600
B3	300	20	5	600
C1	400	30	5	600
C2	500	30	5	600
C3	565	30	5	600
D1	300	30	5	400
D2	300	30	5	800

3 Results and discussion

3.1 Effect of leakage crack width on the migration process

Cases A1–A4 researched the influence of the slot width on the leakage and migration characteristics, with an operating temperature of 300 °C and a leaking molten salt mass of 600 g. Leaking molten salt migrates down and around among the pores of the porous foundation material LECA. Heat is exchanged from the molten salt to the foundation material at the same

time. When the temperature of the molten salt drops to its freezing point, it begins to solidify. During the solidification process, the surrounding LECA granules are bonded together with solid salt to form agglomerates. Fig. 3 gives the agglomerations of solidified salt and LECA along the length and width directions of slot. In general, the agglomerations have a thinner upper part and a thicker lower part, and the migration width along the length of the slot is greater than that along its width. The migration width and migration depth of each case are given in Fig. 4. As the slot width increases from 3 mm to 10 mm with a length of 30 mm, the average migration width of molten salt in LECA increases by 12.1% from 89 mm to 100 mm. The average width along the length of the slot increases from 95 mm to 110 mm and the width along the width of the slot rises from 83 mm to 90 mm. The distances from the top of the agglomerations to the leaking point without salt are between 31 mm and 33 mm, and the migration depth is in the range of 378–400 mm. Therefore, as the width of the slot increases, the molten salt migration depth in LECA changes slightly, and the migration width along the length and width of the slot increases only in a small range.

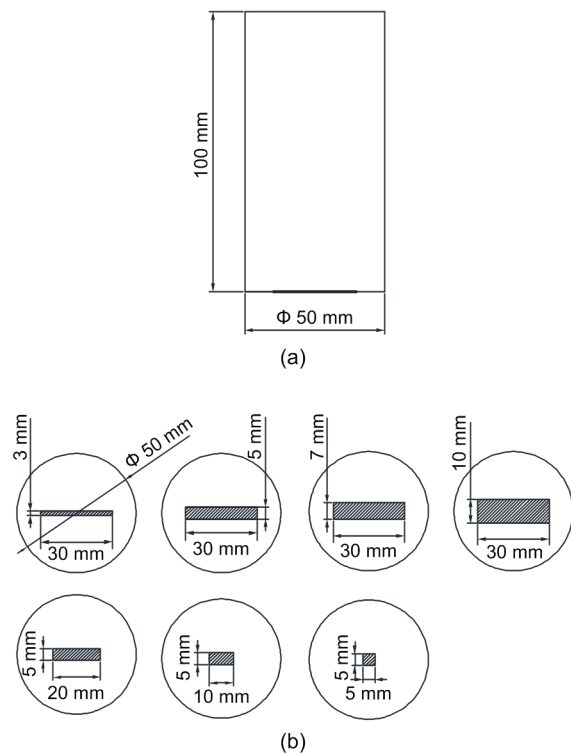


Fig. 2 Diagram of the leaking crucibles with slots at the bottom: (a) side view; (b) vertical view

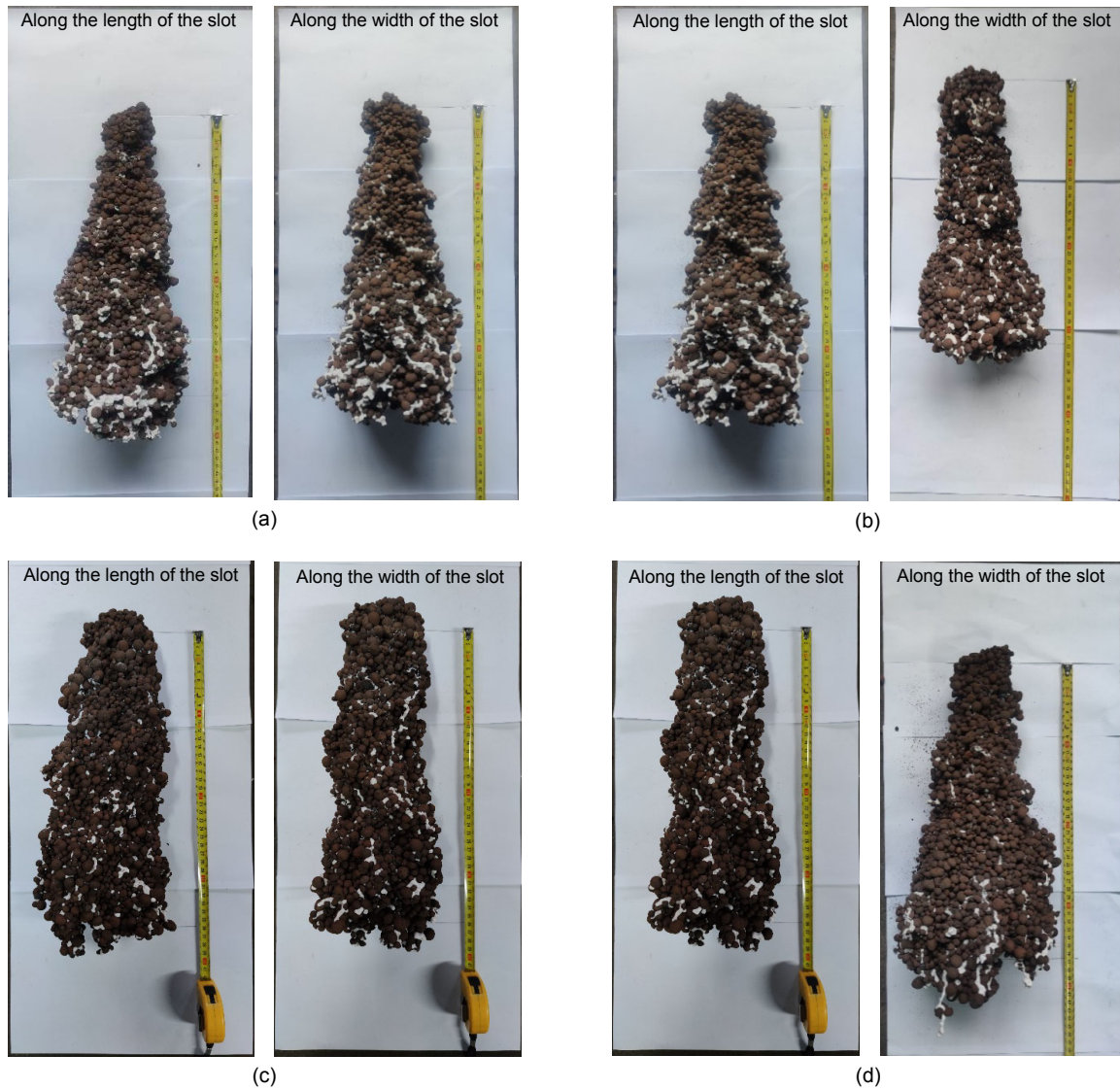


Fig. 3 Agglomerations of LECA and salt with different leakage slot widths: (a) 30 mm×3 mm (case A1); (b) 30 mm×5 mm (case A2); (c) 30 mm×7 mm (case A3); (d) 30 mm×10 mm (case A4)

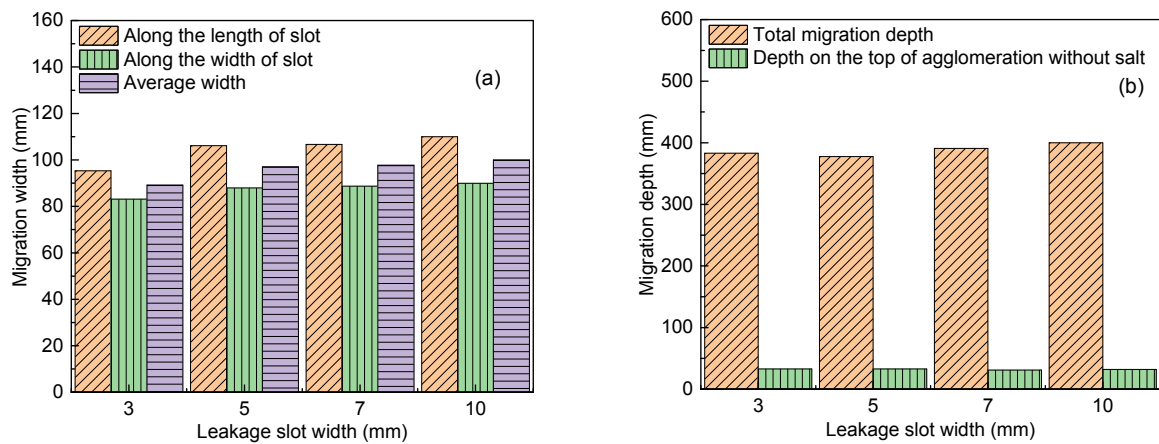


Fig. 4 Molten salt migration characteristics with different leakage slot widths: (a) migration width; (b) migration depth

3.2 Effect of leakage crack length on migration process

The agglomerations of LECA and salt in cases B1–B3 and A2 are shown in Fig. 5. The slot length of case A2 is 30 mm, while those of cases B1–B3 are 5 mm, 10 mm, and 20 mm, respectively. With the same width, the smaller the length of the slot, the greater the difference between the upper and lower width of the agglomerations. When the slot length is 5 mm or 10 mm, the agglomeration shape is similar to a cone. The width of the solid block of LECA and salt

is obviously smaller at the upper part, and the width at the lower part gradually increases. However, the difference between the upper and lower width of the agglomerations is reduced with slots of 20 mm×5 mm and 30 mm×5 mm. As the molten salt migrates downward, it gradually migrates radially at the same time. Fig. 6 shows how the migration width and depth change with the length of slot. As the length increases from 5 mm to 30 mm, the average migration width along its length and width increases by 7.3% and 5.6%, respectively. The molten salt migration depth is reduced by 11.4%, and the distance between the top of

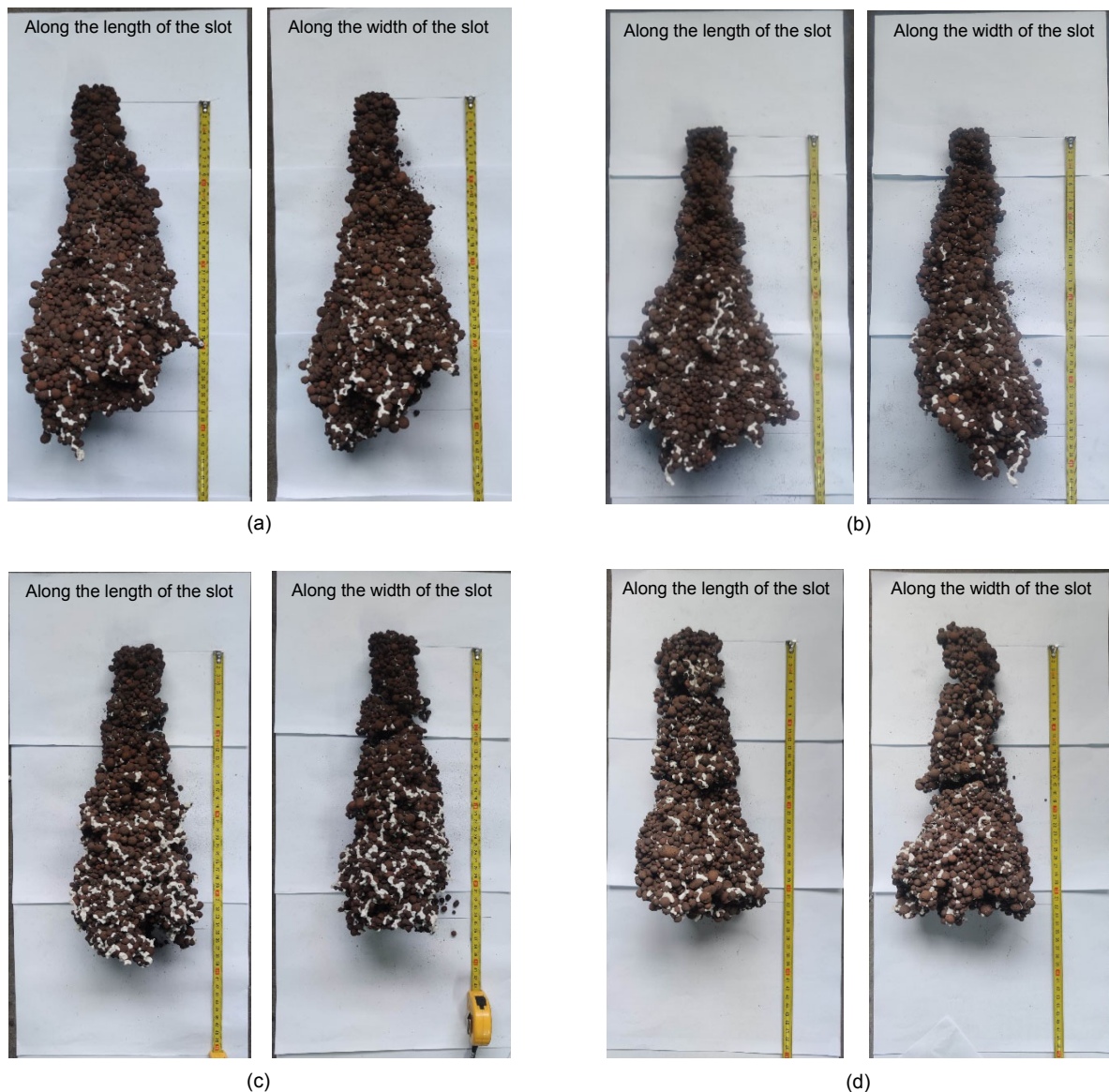


Fig. 5 Agglomerations of LECA and salt with different leakage slot lengths: (a) 5 mm×5 mm (case B1); (b) 10 mm×5 mm (case B2); (c) 20 mm×5 mm (case B3); (d) 30 mm×5 mm (case A2)

the agglomerations and the leaking location also reduces from 45 mm to 30 mm. With an increase in the length of the slot, the agglomeration shape changes markedly, and the molten salt migration width gradually increases, but the migration depth decreases.

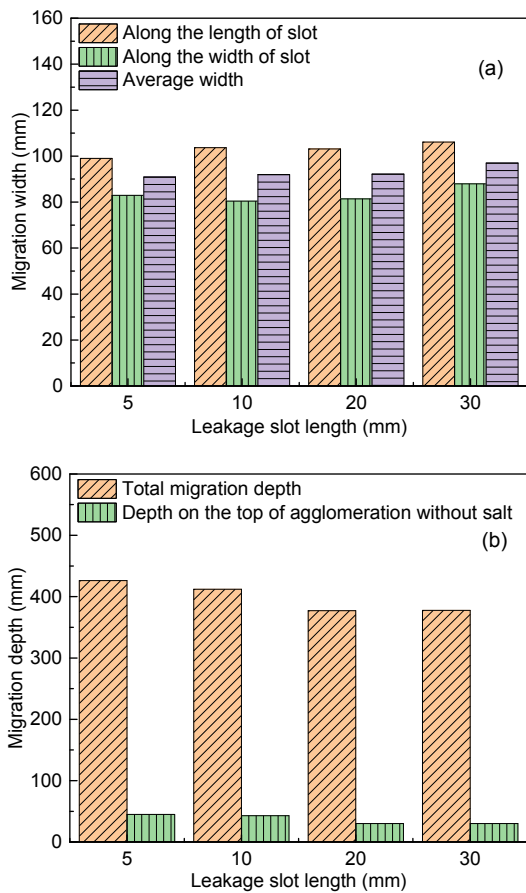


Fig. 6 Molten salt migration characteristics with different leakage slot lengths: (a) migration width; (b) migration depth

3.3 Effect of operating temperature on migration process

The stable thermal temperatures of the porous material under the operating temperatures of 300–565 °C are shown in Fig. 7. As the temperature rises, the drop rate of the foundation material temperature rises with depth. Along with the depth of the foundation, the temperature drop rate gradually decreases, and the temperature difference at the bottom of the foundation is very low. Fig. 8 gives the temperature change of leaking and migration processes with different operating temperatures of molten salt at the

depths of 80 mm and 160 mm of foundation. When the molten salt leaks, the high-temperature fluid quickly migrates within the porous foundation material, and the temperature of the porous material rises quickly. At the tested operating temperatures, the time differences of the temperature rise at the depths of 80 mm and 160 mm are less than 2 s, and the molten salt migrating velocities exceed 0.04 m/s. With the heat transferring from the salt to the porous material, the molten salt temperature first drops rapidly and then slowly stabilizes to the thermal equilibrium temperature. In the first 25 min, when the operating temperatures are 300 °C, 400 °C, and 500 °C, the average temperature drop rates are 3.19 °C/min, 4.75 °C/min, and 5.11 °C/min at the depth of 80 mm, and the values are 2.76 °C/min, 5.70 °C/min, and 5.86 °C/min at the depth of 160 mm, respectively. The temperature change slows down with an average

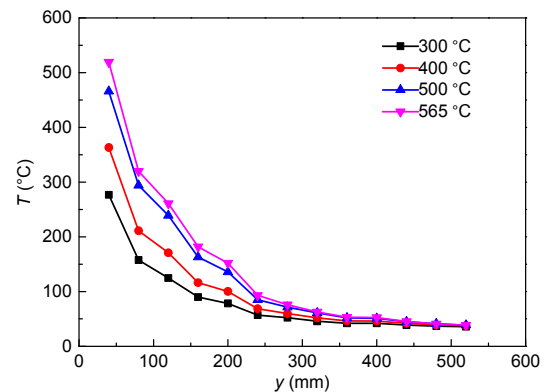


Fig. 7 Thermal equilibrium temperatures of the foundation material with different operating temperatures

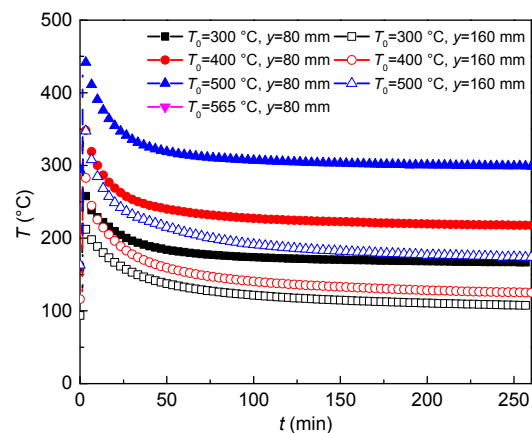


Fig. 8 Temperature evolution of the molten salt leakage and migration processes with different operating temperatures

rate of 0.73–1.06 °C/min from 25 min to 50 min and 0.21–0.47 °C/min from 50 min to 100 min. After 100 min, the temperature gradually stabilizes to the equilibrium temperature.

Fig. 9 shows the agglomerations of LECA and salt under different operating temperatures. With the increase of operating temperature, the height of the agglomeration increases significantly, the degree of looseness increases, and the agglomerations become more columnar. The migration characteristics with operating temperatures of 300–565 °C are given in Fig. 10. There is little change in the migration width

at the operating temperature of 300–500 °C, and the migration width along with different directions of the slot also changes little. However, the migration width at 565 °C is reduced. As the temperature rises, the distance from the agglomeration top to the tank and the total migration depth of molten salt both increase significantly. With an operating temperature of 300 °C, the molten salt migration depth is 378 mm, and the part without solidified molten salt is only 33 mm. When the operating temperature is increased to 500 °C, the migration depth rises to 739 mm with an increase of 95.8%, including a part without solidified

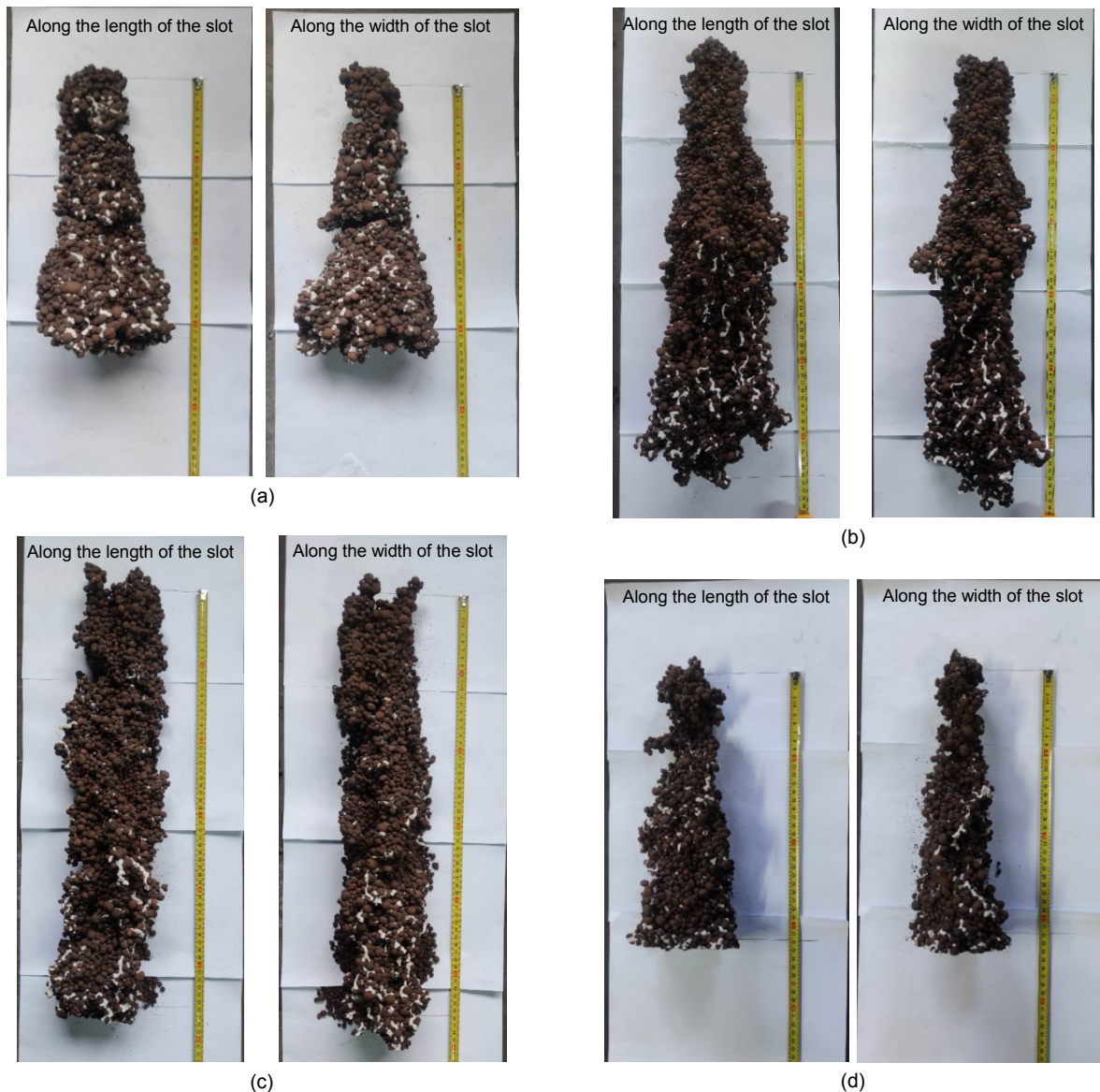


Fig. 9 Agglomerations of LECA and salt with different operating temperatures: (a) 300 °C (case A1); (b) 400 °C (case C1); (c) 500 °C (case C2); (d) 565 °C (case C3)

molten salt of 180 mm. With an operating temperature of 565 °C, the depth where there is no solidified molten salt on the top of agglomeration reaches 435 mm. The migration depth mainly depends on the initial temperature of the molten salt and the foundation temperature distribution. When the operating temperature is high, the high temperature leaking molten salt needs a long path to transfer heat to the foundation material before reaching the freezing point. The operating temperature is the most important factor affecting the molten salt migration depth. According to the temperature values of foundation material after the molten salt migration process in Fig. 8 and the distances from the top of the agglomerations to the leakage positions at different operating temperatures in Fig. 10, the temperature at the molten salt position after the migration process is lower than the molten salt freezing point. It can be inferred that the molten salt flows downward during the migration process until it reaches its freezing point. Therefore,

the salt in the foundation material is completely in the solid phase after the migration process.

3.4 Effect of leakage molten salt mass on migration process

When the leakage molten salt mass varies, the agglomerations of LECA and salt are shown in Fig. 11. It can be seen that with the increase of the leakage molten salt mass, the width of the lower part of the solidified block increases significantly, while the change of the upper part width is small. The migration width and depth changes with the increase of leakage molten salt mass are shown in Fig. 12. As the mass of leakage molten salt increases in the range of 400–800 g, the distance from the top of the molten salt block to the leaking location is basically identical due to the consistent temperature of molten salt and foundation material. The migration depth of molten salt leaking through the slot rises slightly with the increase of leakage molten salt mass, but the molten salt migration width along the radial direction gradually increases. As the mass of the leaked molten salt is 800 g, the average migration width is 107 mm, which is an increase of 23.6% compared to the salt mass of 400 g, where the migration depth only increases by 5.2%.

During the normal operating process, the foundation reaches a thermal stable state with the high-temperature storage tank. After the molten salt leaks, the temperatures of the foundation material with nitrate gradually stabilize to a new equilibrium temperature as the heat transfers between foundation material and salt. Fig. 13 gives the thermal stable temperature distribution of the porous material before and after the molten salt leakage in cases D1, A2, and D2. Due to the same storage tank operating temperature, the equilibrium temperature distributions of these three cases are consistent before molten salt leakage. The results in Fig. 13 show that the stable temperatures of the porous material increase after the molten salt leaking process, especially in the middle layer. Moreover, as the mass of leaking molten salt increases, the equilibrium temperature rises. It is deemed that this increase is caused by the thermal conductivity of the leaking molten salt in the pores of foundation material being greater than that of the air among the foundation material granules.

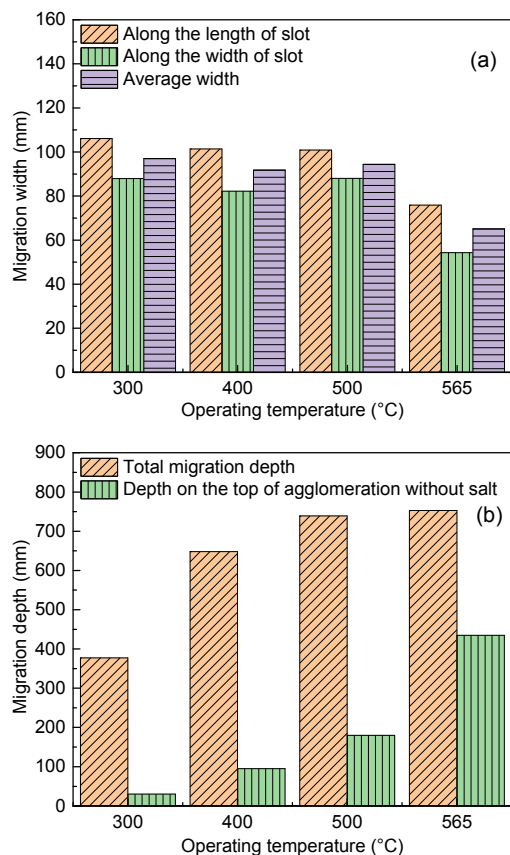
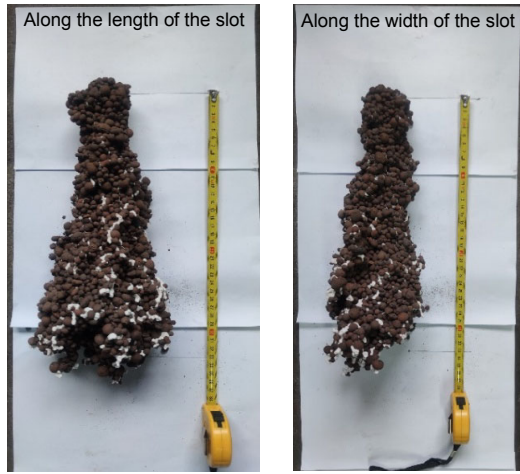
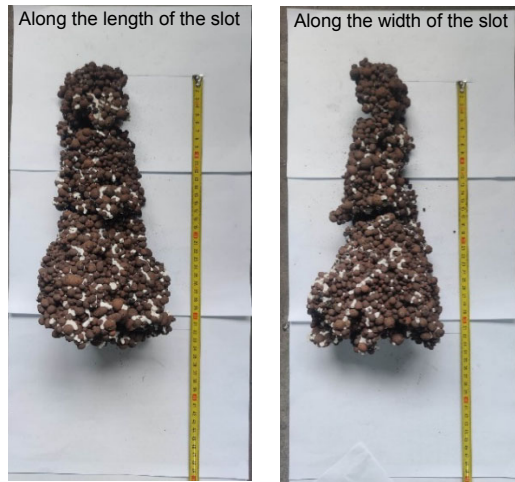


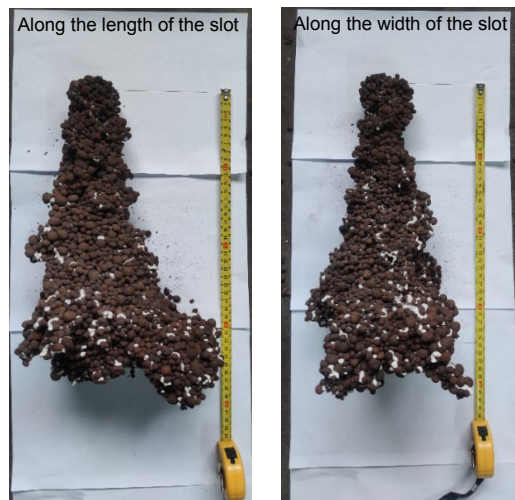
Fig. 10 Molten salt migration characteristics with different operating temperatures: (a) migration width; (b) migration depth



(a)



(b)



(c)

Fig. 11 Agglomerations of LECA and salt with different leakage molten salt masses: (a) 400 g (case D1); (b) 600 g (case A2); (c) 800 g (case D2)

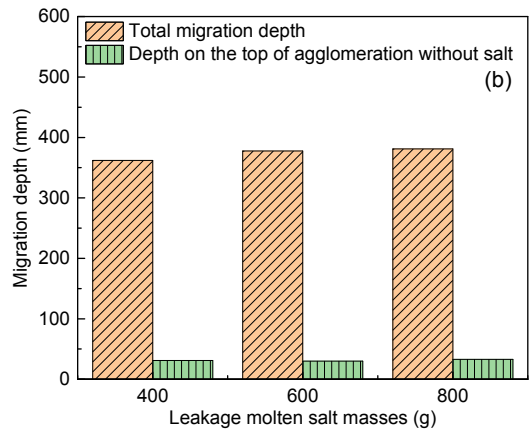
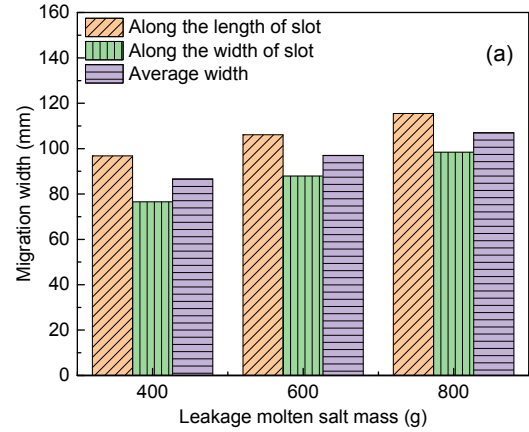


Fig. 12 Molten salt migration characteristics with different leakage molten salt masses: (a) migration width; (b) migration depth

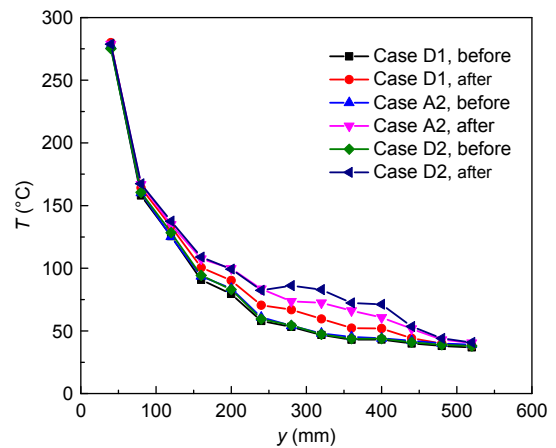


Fig. 13 Thermal equilibrium temperatures of the foundation material before and after molten salt leakage

The effective thermal conductivity of the porous material increases with the increase of thermal conductivity of each component (Zhou et al., 2020b). As

the mass of leaking molten salt increases, the volume fraction of molten salt between the LECA particles increases. The temperature boundary conditions on the top and bottom of the porous foundation material do not change, and the heat flux increases with the increase of the effective thermal conductivity. The temperature gradient of porous material without molten salt on the bottom increases, while the temperature gradient of porous material with molten salt decreases. Therefore, the temperature at the middle of the porous material has risen significantly as the leaking molten salt mass increases.

When the slot width, slot length, and leaking molten salt mass change, the temperature distribution and structural parameters of the foundation material do not change, and the initial temperature of the leakage molten salt is also the same. The molten salt begins to solidify at a similar depth, so the length of agglomerates and molten salt migration depth change little. However, the size of the slot affects the migration path of the molten salt in the radial direction. The greater the mass of the leaking molten salt is, the more molten salt flows in the radial direction. Therefore, the agglomerate shapes of the granules and molten salt under different slot sizes and leaking molten salt masses change significantly, which affects the migration width of the molten salt. In addition, when the operating temperature of the molten salt increases, the molten salt migrating path increases in the foundation material before reaching the freezing point, so the length of the agglomerate and the migration depth of the molten salt significantly increase.

4 Conclusions

This paper experimentally investigated the high-temperature nitrate salt leakage through slots and its migration in porous foundation material accompanying its solidification. The following conclusions can be drawn:

1. When the slot size varies in the range of 3–10 mm width and 5–30 mm length, respectively, the molten salt migration depth and width change slightly, but the width of the upper part of the molten salt and foundation material agglomeration significantly increases with the increase in slot size.

2. The operating temperature is the most critical factor affecting the migration depth when molten salt leaks through slots. As the operating temperature of the storage tank rises from 300 °C to 500 °C, the distance from the top of the agglomeration to the leaking location increases from 30 mm to 180 mm, and the total migration depth increases by 95.8%.

3. The increase of leakage molten salt mass in a certain range has little influence on the molten salt migration depth. The migration width increases with the growth of molten salt mass. As the molten salt mass rises from 400 g to 800 g, the average migration width rises by 23.6%, but the migration depth only increases by 5.2%. Furthermore, the thermal stable temperatures of the porous foundation material after the leaking accident increase with an increase of the leakage molten salt mass.

Contributors

Hua SHI and Hao ZHOU designed the research. Hua SHI, Peng-nan MA, Jian-kang WANG, Hao FANG, and Jia-wei LUO processed the corresponding data. Hua SHI wrote the first draft of the manuscript. Hao ZHOU helped to organize the manuscript. Hua SHI, Hao ZHOU, Peng-nan MA, and Kun-zan QIU revised and edited the final version.

Conflict of interest

Hua SHI, Hao ZHOU, Peng-nan MA, Jian-kang WANG, Hao FANG, Jia-wei LUO, and Kun-zan QIU declare that they have no conflict of interest.

References

- Abdulla A, Reddy KS, 2017. Effect of operating parameters on thermal performance of molten salt packed-bed thermocline thermal energy storage system for concentrating solar power plants. *International Journal of Thermal Sciences*, 121:30-44.
<https://doi.org/10.1016/j.ijthermalsci.2017.07.004>
- Bonilla J, Rodriguez-García MM, Roca L, et al., 2018. Design and experimental validation of a computational effective dynamic thermal energy storage tank model. *Energy*, 152:840-857.
<https://doi.org/10.1016/j.energy.2017.11.017>
- Bremer K, Meinhardt-Wollweber M, Thiel T, et al., 2014. Sewerage tunnel leakage detection using a fibre optic moisture-detecting sensor system. *Sensors and Actuators A: Physical*, 220:62-68.
<https://doi.org/10.1016/j.sna.2014.09.018>
- Chieruzz M, Cerritelli GF, Miliozzi A, et al., 2017. Heat capacity of nanofluids for solar energy storage produced by dispersing oxide nanoparticles in nitrate salt mixture directly at high temperature. *Solar Energy Materials and*

- Solar Cells*, 167:60-69.
<https://doi.org/10.1016/j.solmat.2017.04.011>
- Du BC, He YL, Zheng ZJ, et al., 2016. Analysis of thermal stress and fatigue fracture for the solar tower molten salt receiver. *Applied Thermal Engineering*, 99:741-750.
<https://doi.org/10.1016/j.applthermaleng.2016.01.101>
- Ferri R, Cammi A, Mazzei D, 2008. Molten salt mixture properties in RELAP5 code for thermodynamic solar applications. *International Journal of Thermal Science*, 47(12):1676-1687.
<https://doi.org/10.1016/j.ijthermalsci.2008.01.007>
- Flueckiger S, Yang Z, Garimella SV, 2011. An integrated thermal and mechanical investigation of molten-salt thermocline energy storage. *Applied Energy*, 88(6):2098-2105.
<https://doi.org/10.1016/j.apenergy.2010.12.031>
- Gomes A, Navas M, Uranga N, et al., 2019. High-temperature corrosion performance of austenitic stainless steels type AISI 316L and AISI 321H, in molten Solar Salt. *Solar Energy*, 177:408-419.
<https://doi.org/10.1016/j.solener.2018.11.019>
- Huang J, Zhou ZD, Zhang DS, et al., 2013. A fiber Bragg grating pressure sensor and its application to pipeline leakage detection. *Advances in Mechanical Engineering*, 5:590451.
<https://doi.org/10.1155/2013/590451>
- Im IT, Kim WS, Lee KS, 2001. A unified analysis of filling and solidification in casting with natural convection. *International Journal of Heat and Mass Transfer*, 44(8):1507-1515.
[https://doi.org/10.1016/S0017-9310\(00\)00197-6](https://doi.org/10.1016/S0017-9310(00)00197-6)
- Janz GJ, 1967. *Molten Salts Handbook*. Academic Press, New York, USA.
- Li XL, Xu ES, Song S, et al., 2017. Dynamic simulation of two-tank indirect thermal energy storage system with molten salt. *Renewable Energy*, 113:1311-1319.
<https://doi.org/10.1016/j.renene.2017.06.024>
- Liao ZR, Li X, Wang ZF, et al., 2014. Phase change of molten salt during the cold filling of a receiver tube. *Solar Energy*, 101:254-264.
<https://doi.org/10.1016/j.solener.2014.01.002>
- Lu JF, Ding J, Yang JP, 2010. Solidification and melting behaviors and characteristics of molten salt in cold filling pipe. *International Journal of Heat and Mass Transfer*, 53(9-10):1628-1635.
<https://doi.org/10.1016/j.ijheatmasstransfer.2010.01.033>
- Lu JF, Shen XY, Ding J, et al., 2013. Convective heat transfer of high temperature molten salt in transversely grooved tube. *Applied Thermal Engineering*, 61(2):157-162.
<https://doi.org/10.1016/j.applthermaleng.2013.07.037>
- Ou XX, Zhang X, Lowe T, et al., 2017. X-ray micro computed tomography characterization of cellular SiC foams for their applications in chemical engineering. *Materials Characterization*, 123:20-28.
<https://doi.org/10.1016/j.matchar.2016.11.013>
- Prieto C, Osuna R, Fernández AI, et al., 2016a. Molten salt facilities, lessons learnt at pilot plant scale to guarantee commercial plants; heat losses evaluation and correction. *Renewable Energy*, 94:175-185.
<https://doi.org/10.1016/j.renene.2016.03.039>
- Prieto C, Osuna R, Fernández AI, et al., 2016b. Thermal storage in a MW scale. Molten salt solar thermal pilot facility: plant description and commissioning experiences. *Renewable Energy*, 99:852-866.
<https://doi.org/10.1016/j.renene.2016.07.053>
- Sun H, Wang JQ, Tang ZF, et al., 2020. Assessment of effects of Mg treatment on corrosivity of molten NaCl-KCl-MgCl₂ salt with Raman and infrared spectra. *Corrosion Science*, 164:108350.
<https://doi.org/10.1016/j.corsci.2019.108350>
- Vialle S, Druhan JL, Maher K, 2016. Multi-phase flow simulation of CO₂ leakage through a fractured caprock in response to mitigation strategies. *International Journal of Greenhouse Gas Control*, 44:11-25.
<https://doi.org/10.1016/j.ijggc.2015.10.007>
- Wan ZJ, Wei JJ, Qaisrani MA, et al., 2020. Evaluation on thermal and mechanical performance of the hot tank in the two-tank molten salt heat storage system. *Applied Thermal Engineering*, 167:114775.
<https://doi.org/10.1016/j.applthermaleng.2019.114775>
- Weisbrod N, Niemet MR, Rockhold ML, et al., 2004. Migration of saline solutions in variably saturated porous media. *Journal of Contaminant Hydrology*, 72(1-4):109-133.
<https://doi.org/10.1016/j.jconhyd.2003.10.013>
- Wu JQ, Ding J, Lu JF, et al., 2017. Migration and phase change phenomena and characteristics of molten salt leaked into soil porous system. *International Journal of Heat and Mass Transfer*, 111:312-320.
<https://doi.org/10.1016/j.ijheatmasstransfer.2017.04.002>
- Wu M, Xu C, He YL, 2016. Cyclic behaviors of the molten-salt packed-bed thermal storage system filled with cascaded phase change material capsules. *Applied Thermal Engineering*, 93:1061-1073.
<https://doi.org/10.1016/j.applthermaleng.2015.10.014>
- Xu L, Stein W, Kim JS, et al., 2018. Three-dimensional transient numerical model for the thermal performance of the solar receiver. *Renewable Energy*, 120:550-566.
<https://doi.org/10.1016/j.renene.2017.12.055>
- Yang XP, Yang XX, Qin FGF, et al., 2016. Experimental investigation of a molten salt thermocline storage tank. *International Journal of Sustainable Energy*, 35(6):606-614.
<https://doi.org/10.1080/14786451.2014.930465>
- Yao F, Bi QC, Dong XY, 2018. Convective heat transfer of high temperature molten salt flowing across tube bundles of steam generator in a solar thermal plant. *Applied Thermal Engineering*, 141:858-865.
<https://doi.org/10.1016/j.applthermaleng.2018.06.004>
- Yin HB, Ding J, Jiang RH, et al., 2017. Thermocline characteristics of molten-salt thermal energy storage in porous

- packed-bed tank. *Applied Thermal Engineering*, 110:855-863.
<https://doi.org/10.1016/j.applthermaleng.2016.08.214>
- Yuan F, Li MJ, Ma Z, et al., 2018. Experimental study on thermal performance of high-temperature molten salt cascaded latent heat thermal energy storage system. *International Journal of Heat and Mass Transfer*, 118:997-1011.
<https://doi.org/10.1016/j.ijheatmasstransfer.2017.11.024>
- Zafari M, Panjepour M, Emami MD, et al., 2015. Microtomography-based numerical simulation of fluid flow and heat transfer in open cell metal foams. *Applied Thermal Engineering*, 80:347-354.
<https://doi.org/10.1016/j.applthermaleng.2015.01.045>
- Zhang YY, Wu JQ, Wang WL, et al., 2019. Experimental and numerical studies on molten salt migration in porous system with phase change. *International Journal of Heat and Mass Transfer*, 129:397-405.
<https://doi.org/10.1016/j.ijheatmasstransfer.2018.09.122>
- Zhou H, Shi H, Zhang JK, et al., 2020a. Experimental and numerical investigation of temperature distribution and heat loss of molten salt tank foundation at different scales. *Heat and Mass Transfer*, 56(10):2859-2869.
<https://doi.org/10.1007/s00231-020-02905-x>
- Zhou H, Shi H, Lai ZY, et al., 2020b. Migration and phase change study of leaking molten salt in tank foundation material. *Applied Thermal Engineering*, 170:114968.
<https://doi.org/10.1016/j.applthermaleng.2020.114968>